J Mater Sci (2007) 42:6074–6086
DOI 10.1007/s10853-006-1159-4

Spectroscopic characterization of tungstated zirconia prepared by equilibrium adsorption from hydrogen peroxide solutions of tungsten(VI) precursors

Margarita Kantcheva · Cevryie Koz

Received: 19 July 2006 / Accepted: 17 October 2006 / Published online: 16 April 2007

Abstract Two series of WO_x/ZrO_2 samples are prepared by equilibrium adsorption from H_2O_2 solutions at pH 1.8 containing two different precursor anions, $[W_2O_3(O_2)_4(H_2O)_2]^{2-}$ and $[H_2W_{12}O_{40}]^{6-}$. The starting material is amorphous zirconium oxyhydroxide. The maximum W densities obtained are larger than that reported in the literature for systems synthesized by the same method using aqueous non-peroxide solutions. In the case of the metatungstate precursor, this increase is attributed to the generation of additional anchoring sites by interaction between the amorphous support and H_2O_2. The high uptake achieved when the peroxo complex is used as a precursor is a result of both the $ZrO_x(OH)_{4-2x}$–H_2O_2 interaction and low nuclearity of the adsorbing anion. The materials are characterized by XRD, DR–UV–vis, Micro-Raman and FT-IR spectroscopy. The surface acidities of samples with identical W loading prepared by equilibrium adsorption from the $[H_2W_{12}O_{40}]^{6-}$–H_2O_2 system and by impregnation with aqueous solution of ammonium metatungstate are investigated by FT-IR spectroscopy of CO adsorbed at 80 K.

Introduction

Among the zirconia-supported systems, tungsten oxide-based catalysts, have received a great deal of attention, because they are attractive as catalysts for the reactions of isomerization of light alkanes [1–7] and selective catalytic reduction of nitrogen oxides with hydrocarbons [8, 9]. The catalytic properties of these oxide systems depend strongly on the WO_x surface density, which can be varied by changing the content of the active oxide phase and the catalyst treatment temperature [1–9].

The WO_x/ZrO_2 catalysts are usually prepared by impregnating hydrous zirconium oxyhydroxide, $ZrO_x(OH)_{4-2x}$, with aqueous solutions of ammonium metatungstate (AMT) [2–4, 6–13] or by coprecipitation [5] followed by calcination in air. In general, the equilibrium adsorption procedures allow better dispersion of the active phase and this method has been used by Valigi and coworkers [13–16] to prepare various zirconia-based catalysts starting from amorphous $ZrO_x(OH)_{4-2x}$. These authors demonstrated the role of the solution pH in determining both the adsorption properties of the support and the predominant ionic form of the precursor. The latter is particularly important for tungsten, which can exist as monomeric species, $[WO_4]^{2-}$, in solutions at pH higher than 8, whereas oligomeric species, $[H_xW_yO_z]^{n-}$, are formed in acidic medium [17]. The adsorption of anionic species on zirconia is favored in solutions with a pH below 6.7 [18], the PZC of zirconia [14]. The large isopolyanions formed under these conditions suffer diffusion limitation into the micropores of the amorphous zirconium oxyhydroxide and can be adsorbed only on the external surface of the support grains [14]. Therefore, the application of anionic precursors with reduced nuclearity for synthesis of zirconia-supported WO_x species can increase the ion-exchange capacity of the support and improve the dispersion of the adsorbed species. Low-condensed anionic oxoperoxometalate species can be generated dissolving metavanadates [19], polyoxomolybdates or -tungstates [20] in an excess of hydrogen peroxide at pH 0.5–2. We used this experimental fact to develop a ''peroxo route'' for synthesis of VO_x/ZrO_2 catalysts involving equilibrium adsorption of

M. Kantcheva (✉) · C. Koz
Laboratory for Advanced Functional materials, Department of Chemistry, Bilkent University, 06800 Bilkent, Ankara, Turkey
e-mail: margi@fen.bilkent.edu.tr

peroxovanadium(V) ions on stabilized zirconia in aqueous solutions at low pH [21]. Compared to the non-peroxide systems, the adsorption of vanadium(V) peroxo ions resulted in approximately 2-fold increase of the loading and better dispersion of the VO_x species deposited on zirconia. Recently, Loridant et al. [22] used similar scheme in the preparation of tungstated zirconia by anionic exchange of peroxotungstate species with hydroxyl groups of $ZrO_x(OH)_{4-2x}$ at low pH.

This paper presents a spectroscopic study of tungstated zirconias obtained by equilibrium adsorption using amorphous $ZrO_x(OH)_{4-2x}$ and aqueous solutions prepared by dissolving $(NH_4)_2WO_4$ and AMT in H_2O_2 as precursors. The structural characteristics of samples with identical tungsten loading obtained by the ''peroxo route'' and impregnation have been compared.

Experimental

Sample Preparation

Amorphous $ZrO_x(OH)_{4-2x}$ was prepared by hydrolysis of $ZrCl_4$ (Merck, for synthesis) with concentrated (25%) solution of ammonia as already described [23]. After washing (negative test for Cl^- ions), the precipitate was dried at 383 K in air for 24 h. According to XRD, the solid (specific surface area of 298 m^2/g) was amorphous. This material (denoted as ZrO_2-383) was used to prepare the tungsten-containing samples. Two preparation procedures were employed:

(i) ''Peroxo route'' involving equilibrium adsorption from aqueous solutions prepared by dissolving two different W-containing compounds in cold 30% H_2O_2 (Merck, without stabilizers) at pH = 1.8 adjusted by addition of HNO_3. The solutions with concentrations of 0.05, 0.50 and 0.75 W mol/L containing the dimeric oxodiperoxo complex, $[W_2O_3(O_2)_4(H_2O)_2]^{2-}$, were obtained using $(NH_4)_2WO_4$ (Aldrich) as a precursor [20]. These solutions were denoted as ''solutions 1''. The ''solutions 2'' with concentrations ranging from 0.05 to 0.90 W mol/L were prepared by dissolving ammonium metatungstate $[(NH_4)_6H_2W_{12}O_{40}\cdot 18H_2O$, Fluka] (AMT). No precipitate formation from the precursor solutions 1 and 2 was observed within a period of 36 h. The tungsten-containing samples were obtained by suspending an amount of ZrO_2-383 in a large volume of the desired solution for 24 h upon stirring at room temperature. Then the solid was separated from the solution, washed several times with deionized water and dried at 383 K for 24 h followed by calcination for 4 h at 923 K. The samples are designated as cWZ-1-T and cWZ-2-T, where 1 and 2 indicate the precursor solutions 1 and 2, c stands for their concentration and T is the temperature of thermal treatment.

(ii) Impregnation: the sample was prepared by suspending for 24 h ZrO_2-383 in aqueous solutions containing an amount of AMT sufficient to obtain calcined material with loading of 19.0 wt% W. Water was removed from the suspension by evaporation. The sample was submitted to the same thermal treatment as described above. The material obtained is denoted as WZ-I.

Characterization techniques

Chemical analysis

Tungsten in the as prepared samples (cWZ-1-383 and cWZ-2-383) was leached out in an excess of 2 M NaOH. The calcined samples were fused with $KHSO_4$ and then dissolved in water. The tungsten content was determined spectrophotometrically by the thiocyanate method [24, 25]. The W surface densities are expressed as the number of atoms per nanometer square of surface area (W/nm^2).

Surface area measurements, X-ray diffraction and DR–UV–vis spectroscopy

The BET surface areas of the samples (dehydrated at 523 K) were measured by nitrogen adsorption at 77 K using Monosorp apparatus from Quantachrome. XRD analysis was performed on a Rigaku Miniflex diffractometer with Ni-filtered Cu Kα radiation under ambient conditions. DR–UV–vis spectra were obtained under ambient conditions with a fiber optic spectrometer AvaSpec-2048 (Avantes) using WS-2 as a reference.

Micro-Raman spectroscopy

The micro-Raman spectra were recorded on a LabRam confocal Raman microscope with a 300 mm focal length. The spectrometer is equipped with a HeNe laser operated at 20 mW, polarized 500:1 with a wavelength of 623.817 nm, and 1024 × 256 element CCD camera. The signal collected was transmitted through a fiber optic cable into a grating with 600 g/mm spectrometer.

FT-IR spectroscopy

The FT-IR spectra were recorded using a Bomem Hartman & Braun MB-102 model FT-IR spectrometer with a liquid-nitrogen cooled MCT detector at a resolution of 4 cm^{-1}

(128 scans). The self-supporting discs (0.035 g/cm^2) were activated in the IR cell (Xenonum Scientific) equipped with a cryogenic apparatus by heating for 1 h in a vacuum at 723 K, and in oxygen (100 mbar, passed through a trap cooled in liquid nitrogen) at the same temperature, followed by evacuation for 1 h at 723 K. The CO (99.95%, BOC, passed through a trap cooled in liquid nitrogen) was introduced at 77 K in increasing amounts in the pressure range 0–25 mbar.

Results

Tungsten species in the solutions

Figure 1a shows the Raman spectra of the prepared precursor solutions with concentrations of 0.50 W mol/L. The spectrum of the H_2O_2 solution (spectrum a) and that of non-peroxidic aqueous solution of AMT with concentration of 0.50 W mol/L (spectrum d), both at pH 1.8, are also included. The strong band at 879 cm^{-1} in the former spectrum corresponds to the δ_s(O-O) mode of hydrogen peroxide [26] whereas the signal at 1050 cm^{-1} belongs to the NO_3^- ion [27] from the HNO_3 used for the pH adjustment. The observed Raman features of solution 1 (Fig. 1a, spectrum b) agree well with those of the $[W_2O_3(O_2)_4(H_2O)_2]^{2-}$ ion reported in the literature [28]. The band at 965 cm^{-1} corresponds to the ν(W=O) mode of the dimeric oxo-diperoxo species. The shoulder at 860 cm^{-1} of the strong Raman line at 873 cm^{-1} (due to the presence of excess H_2O_2) is characteristic of the ν(O-O) vibration. The bands at 620 and 562 cm^{-1} are assigned to the $\nu_{as}[W(O_2)]$ and $\nu_s[W(O_2)]$ modes, respectively. The signal at 325 cm^{-1} is characteristic of the W-OH_2 vibration. The band at 1050 cm^{-1} and the weak component at 720 cm^{-1} correspond to the NO_3^- ions. The spectrum of solution 2 (Fig. 1a, spectrum c) is identical with that of the non-peroxide solution of AMT (Fig. 1a, spectrum d). The strong band at 879 cm^{-1} is due to the solvent H_2O_2. The signals at 979, 968, 945 and 898 cm^{-1} are characteristic of the metatungstate ion, $[(H_2)W_{12}O_{40}]^{6-}$ [15]. The spectral features of the AMT-H_2O_2 system do not change within a period of 24 h. It can be concluded that under these conditions, the main tungsten species in solution 2 are the metatungstate ions and no W(VI) preoxo species are generated under these conditions. The spectra of the remaining H_2O_2 solutions of the starting tungsten compounds with concentrations different from 0.50 W mol/L display the same Raman features as described above with band intensities varying with the concentrations.

Figure 1b shows the Raman spectra of the peroxo solutions in contact with the hydrous zirconia after the equilibration for 24 h. There are differences between the equilibrated and the starting solutions that need to be described. In the case of the equilibrated $ZrO_x(OH)_{4-2x}$–H_2O_2 system, the strong signal at 879 cm^{-1} is absent in the spectrum of the solution (compare spectra a and a′ in Fig. 1), which indicates complete decomposition of the H_2O_2. The Raman spectrum of the solution contains bands at 984, 944 and 305 cm^{-1}. This spectrum is very similar to the that of aqueous solution of $ZrO(NO_3)_2$ (not shown) which suggests that hydrated ZrO^{2+} ions are formed during

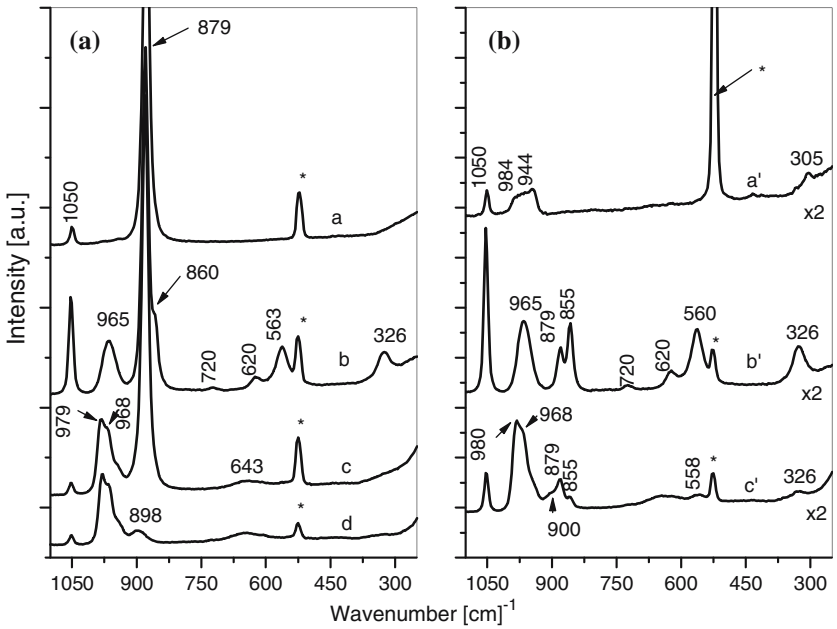

Fig. 1 Panel **a**: Raman spectra of solutions at pH 1.8 of (a) 30 wt% H_2O_2, (b) 0.50 M $(NH_4)_2WO_4$ in 30 wt% H_2O_2 (solution 1), (c) 0.50 W mol/L of AMT in 30 wt% H_2O_2 (solution 2), and (d) 0.50 W mol/L of AMT in H_2O. Panel **b**: Raman spectra of filtrates obtained after 24 h of equilibration with $ZrO_x(OH)_{4-2x}$ at pH 1.8: (a′) 30 wt% H_2O_2, (b′) 0.50 M $(NH_4)_2WO_4$ in 30 wt% H_2O_2 (solution 1), (c′) 0.50 W mol/L of AMT in 30 wt% H_2O_2 (solution 2). The Y scale of the plot in panel **b** is extended by a factor of 2 relative to that in panel **a**. The signal indicated by asterisk belongs to the Si substrate used to record the spectra

the interaction between the hydrous zirconia and H_2O_2. The presence of dissolved Zr^{4+} ions in the solution in equilibrium with the ZrO_2-383 sample has been proven qualitatively by precipitation with NH_3 solution. The Raman spectra of the equilibrated solutions 1 and 2 (Fig. 1b, spectra b′ and c′) show strong decrease in the intensity of the band at 879 cm^{-1} corresponding to the ν(O-O) mode of the excess H_2O_2. This leads to the conclusion that compared to the W-free solution in equilibrium with the ZrO_2-383 sample (Fig. 1b, spectrum a) the degradation of H_2O_2 in the presence of W(VI) anions occurs to a smaller extent. Most probably, the adsorbed tungsten species block some of the active sites of hydrous zirconia, which are involved in the H_2O_2 decomposition. The ZrO^{2+} ion cannot be detected under these conditions because its characteristic bands are covered by the strong signals of the W(VI) peroxo species and metatungstate ions. The traces b′ and c′ in Fig. 1b show that the intensities of the bands of the $[W_2O_3(O_2)_4(H_2O)_2]^{2-}$ and metatungstate ions have decreased because of the ion exchange (compare with spectra b and c in Fig. 1a). The spectrum of the equilibrated solution 2 contains weak bands at 855, 558 and 326 cm^{-1} characteristic of the $[W_2O_3(O_2)_4(H_2O)_2]^{2-}$ ion [28] (see also spectra b and b′). Since no such signals are present in solution 2 before the contact with the hydrous zirconia (Fig. 1a, spectrum c), we can infer that the formation of W(VI) dimeric oxo-diperoxo complex from AMT is possible at a specific concentration ratio $[H_2O_2]/[W^{6+}]$ different from that of the starting solution.

From these results, it can be concluded that the adsorbing species in solution 1 are the $[W_2O_3(O_2)_4(H_2O)_2]^{2-}$ ions, whereas the equilibrated solution 2 contains metatungstate ions as the major component and small amount of the $[W_2O_3(O_2)_4(H_2O)_2]^{2-}$ species.

As prepared samples

Tungsten uptake

Figure 2 shows the variation of the W uptake and surface density as a function of the concentration of the precursor solutions expressed as W mol/L. The W loading of the samples prepared from solutions 1 is higher than that of the samples obtained from solutions 2 (see also Table 1). Obviously, the uptake depends on the size of the adsorbing ions. In both cases, the uptake shows little dependence on the concentration of the precursor solutions and reaches a plateau for values larger than 0.50 and 0.75 W mol/L for solutions 1 and 2, respectively. The surface densities were calculated based on the surface area of the ZrO_2-383 support assuming that the latter was little affected by the W deposition. They lie in the range of 3.4–3.5 and 2.4–2.6 W/nm^2 for cWZ-1-383 and cWZ-2-383 samples, respectively.

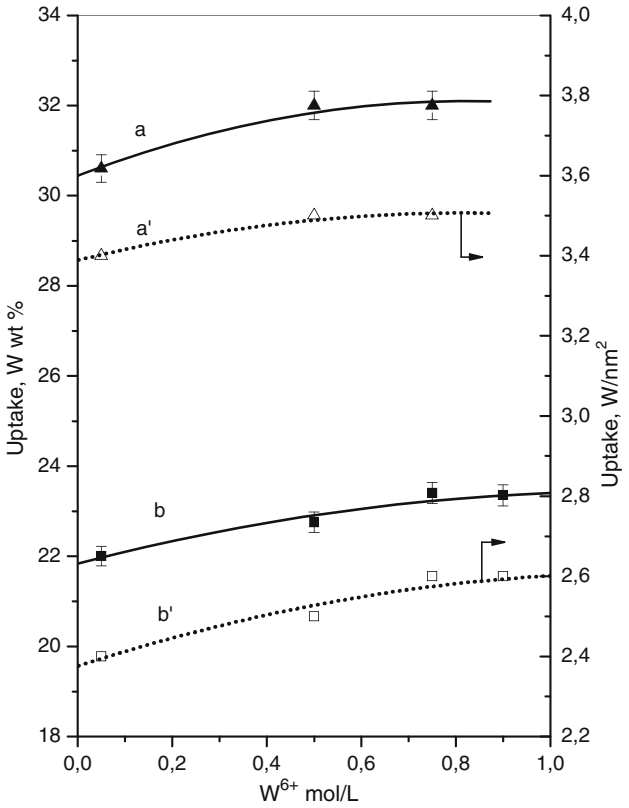

Fig. 2 Tungsten loading (wt%) and surface concentration (W atoms/nm^2) of the as prepared samples as a function of the solution concentration (W mol/L): (a) and (a′) samples cWZ-1-383; (b) and (b′) samples cWZ-2-383

Table 1 W content, absorption edge position and number of nearest W atoms for the as prepared samples

Sample	W wt%	Surface density W/nm^2	E_{edge} eV	N_w
0.05WZ-1-383	30.6	3.4	3.57	4.0
0.50WZ-1-383	32.0	3.5	3.43	4.3
0.75WZ-1-383	32.2	3.5	3.42	4.4
0.05WZ-2-383	22.0	2.4	3.50	4.2
0.50WZ-2-383	22.8	2.5	3.48	4.2
0.75WZ-2-383	23.4	2.6	3.48	4.2
0.90WZ-2-383	23.3	2.6	3.48	4.2

DR–UV–vis Spectroscopy

The absorption spectra of the cWZ-383 samples are shown in Fig. 3. All samples exhibit absorption band at around 278–293 nm corresponding to charge-transfer (CT) transitions in W-O-W units of oligomeric tungstates [3, 4, 10, 12, 29]. The growth in intensity of this band (particularly for the cWZ-1-383) indicates increasing degree of condensation with increasing W loading. The absorption edge

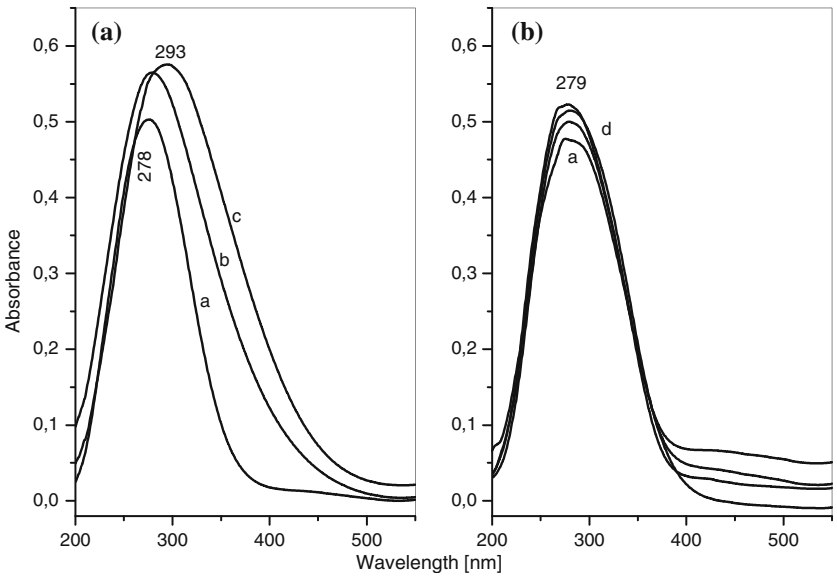

Fig. 3 DR–UV–vis spectra of the as prepared samples. Panel **a**: (a) 0.050WZ-1-383, (b) 0.50WZ-1-383, and (c) 0.75WZ-1-383. Panel **b**: (a) 0.050WZ-2-383, (b) 0.50WZ-2-383, (c) 0.75WZ-2-383 and (d) 0.90WZ-2-383

is clearly shifted towards higher wavelengths for samples 0.50WZ-1-383 and 0.75WZ-1-383 (Fig. 3a, spectra b and c) indicating presence probably of WO_3. In contrast, the spectra of the samples of the cWZ-2-383 series (Fig. 3b) may reflect high dispersion of the WO_x species.

Weber [30] proposed an empirical linear correlation between the number of next nearest Mo neighbors (N_{Mo}) for Mo-O compounds and supported MoO_x species and the value of the absorption edge energy (E_{edge}). Similar correlation between N_W and E_{edge} was found for zirconia-supported WO_x species [3, 12]. The absorption edge energy can be determined by a linear extrapolation to absorption equal zero in $(\alpha h\nu)^2$ versus $h\nu$ plots, where α is the absorbance and $h\nu$ is the energy of the incident photon [3, 12, 30]. This method allows evaluating the average size of dispersed WO_x domains. Using the same reference values as Iglesia et al. [3, 12] we have calculated the N_W values for the two sample series and the results are summarized in Table 1. The absorption edge energies of the cWZ-1-383 samples decrease increasing the loading. This indicates that average size of the WO_x clusters increases. In the case of the cWZ-2-383 samples, the absorption edge energy levels off for loading higher than 2.4 W/nm^2. The average size of the WO_x domains of the two sample series is comparable to that of AMT (N_W = 4 [3, 12]).

Micro-Raman Spectroscopy

The Raman spectrum (Fig. 4) of the amorphous zirconium oxyhydroxide (sample ZrO_2-383) contains a broad band

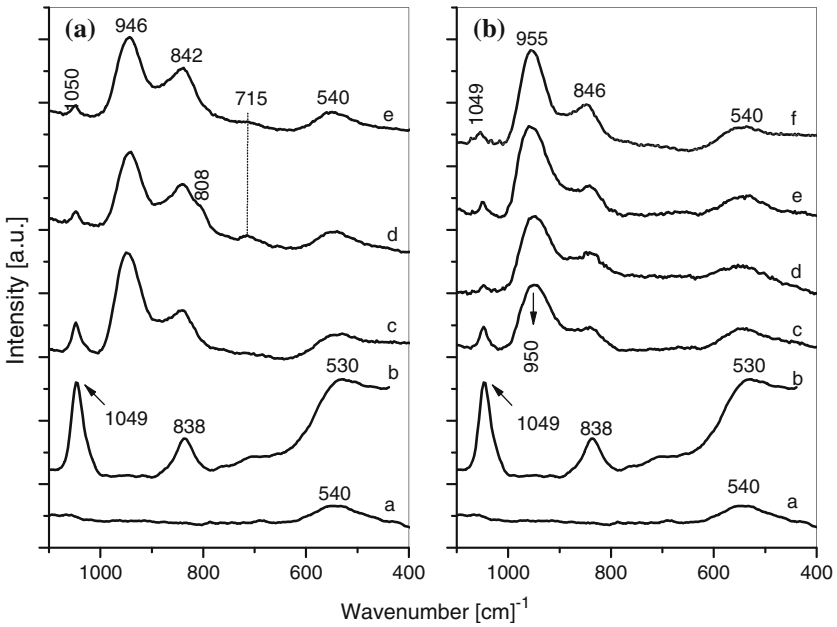

Fig. 4 Raman spectra of the as prepared samples. Panel **a**: (a) ZrO_2-383, (b) ZrO_2-383 treated with 30 wt% H_2O_2 for 24 h, (c) 0.050WZ-1-383, (d) 0.50WZ-1-383, and (e) 0.75WZ-1-383. Panel **b**: (a) ZrO_2-383, (b) ZrO_2-383 treated with 30 wt% H_2O_2 for 24 h, (c) 0.050WZ-2-383, (d) 0.50WZ-2-383, (e) 0.75WZ-2-383 and (f) 0.90WZ-2-383. The spectra are normalized to the band at 540 cm^{-1} of the ZrO_2-383 sample

with maximum 540 cm^{-1}, which is assigned to superimposed Zr-O vibrations in ring structures and Zr–O–Zr bending mode between adjacent ZrO polyhedra [31]. Treatment of the ZrO_2-383 sample with 30% H_2O_2 for 24 h at pH 1.8 causes the appearance of intense bands at 1049, 838 and 530 cm^{-1} (Fig. 4a and b, spectra a). The former band reveals presence of adsorbed NO_3^- species [10]. The maximum at 838 cm^{-1} is characteristic of peroxo [ν(O-O)] vibration and the broad, strong band at 530 cm^{-1} is attributed to the superimposed $\nu_{as}[Zr(O_2)]$ and $\nu_s[Zr(O_2)]$ modes of peroxozirconium(IV) species, respectively [32]. Most probably, these species are formed on the amorphous zirconia as intermediates during the decomposition of H_2O_2.

Comparison of the Raman spectra of the cWZ-383 samples of the two series with that of the H_2O_2-treated ZrO_2-383 (Fig. 4) shows strong decrease in the intensity of the band at 530 cm^{-1} relative to that at 842–846 cm^{-1}. This suggests that the peroxozircinium(IV) species, if present, are formed in a smaller amount. It seems that the samples do not contain W(VI) peroxo species because the spectra do not show a signal at 560–620 cm^{-1} characteristic of the peroxo structural unit $W(O_2)$ [28]. The nitrate band is detected in the spectra of the samples of the two series being most intense on the materials prepared from the most diluted solutions (samples 0.05WZ-1-383 and 0.05WZ-2-383). This result indicates that a competitive adsorption between the NO_3^- and the W-containing species takes place.

The spectra of the cWZ-1-383 samples exhibit two maxima at 946 and 842 cm^{-1} (Fig. 4a). The former band is assigned to the W=O stretching modes, whereas the band at 842 cm^{-1} is attributed to the W-O-W vibrations of hydrated oligomeric WO_x species [10, 11, 13]. This assignment is in agreement with the DR–UV–vis data according to which the average degree of aggregation of the WO_x clusters is close to that of AMT. The weak band at 715 cm^{-1} and the shoulder at 808 cm^{-1} in the spectrum of the sample 0.50WZ-1-383 reveal formation of some crystalline WO_3 [10–12]. The latter compound is present also in the 0.75WZ-1-383 sample, which is evident by the appearance of a weak signal at 715 cm^{-1}. The band profile of the samples of the cWZ-2-383 series (Fig. 4b) is similar to that of the cWZ-1-383 samples. The signal at 950 cm^{-1} in the spectrum of the 0.05WZ-2-383 sample shifts slightly to a higher frequency as the W loading increases. No microcrystalline WO_3 is detected in all cWZ-2-383 materials.

Calcined samples

Physico-chemical characterization

Table 2 summarizes the physico-chemical characteristics of the calcined samples. The tungsten loading of the as prepared and calcined samples is similar suggesting that the dried materials contain hydrated WO_x species ($WO_x \cdot nH_2O$). During the calcination, the loss of water from the latter partially offsets the weight loss of the amorphous zirconium oxyhydroxide. The sample prepared by impregnation has been also included in Table 2 to compare with the ion-exchanged materials. The surface areas of the zirconia-supported WO_x samples are larger than that of pure zirconia. The increase of the surface area after the deposition of WO_x species is well documented in the literature [3, 4, 7, 10, 13]. It is attributed to a reduction of the surface mobility of zirconia by the WO_x overlayer formed [10]. The surface areas of the cWZ-2-923 samples decrease as the loading exceeds 5.3 W/nm^2 but they remain higher than those of the cWZ-1-923 samples. The saturation limit for surface coverage with tungsten in dispersed form is estimated to be ~4–6 atoms/nm^2 [10, 12, 13, 33, 34]. It is apparent from Table 2 that the W surface densities of the cWZ-1-923 samples exceed this value, whereas the W surface densities for the 0.05WZ-2-923 and 0.50WZ-2-923 samples lie in the saturation limit. The W loading of the impregnated WZ-I and 0.05WZ-2-923 samples is identical. However, the surface area of the former is considerably lower than that of the ion-exchanged material.

Table 2 Tungsten content and some characteristics of the samples calcined at 923 K

Sample	W wt%	S_{BET} m^2/g	Surface density W/nm^2	E_{edge} eV	N_W	XRD
ZrO_2-923	-	56	-	-	-	m-ZrO_2
0.05WZ-1-923	30.1	114	8.6	-	-	t-ZrO_2 + WO_3
0.50WZ-1-923	31.8	102	10.2	-	-	t-ZrO_2 + WO_3
0.75WZ-1-923	31.6	99	10.4	-	-	t-ZrO_2 + WO_3
0.05WZ-2-923	21.7	141	5.0	3.32	4.6	t-ZrO_2
0.50WZ-2-923	22.5	140	5.3	3.32	4.6	t-ZrO_2
0.75WZ-2-923	23.1	131	5.8	3.29	4.7	t-ZrO_2 + WO_3
0.90WZ-2-923	22.9	129	5.8	3.30	4.6	t-ZrO_2 + WO_3
WZ-I	19.0	127	4.9	3.33	4.6	t-ZrO_2

m: monoclinic; t: tetragonal

The X-ray diffraction patterns for the samples studied indicate that the incorporation of WO_x species stabilizes the tetragonal phase of zirconia. This result agrees with the observed effect of the surface WO_x compounds on the fraction of tetragonal phase [3–5, 7, 10, 13]. All cWZ-1-923 samples contain crystalline WO_3. This compound is detected also in the 0.75WZ-2-923 and 0.90WZ-2-923 samples.

The absorption edge energies of the cWZ-2-923 samples (Table 2) do not change considerably with increase in the surface density and remain higher than those measured for WO_3 (2.59 eV [3, 12]). Compared to the as prepared samples (Table 1), the sizes of the WO_x domains have increased after the crystallization of zirconia. Because all samples of the cWZ-923 series contain considerable amount of WO_3 detectable by XRD, the determination of the absorption edge position is not reliable.

Micro-Raman Spectroscopy

The Raman spectra of the cWZ-1-923 samples (Fig. 5a) exhibit strong bands due to crystalline WO_3 [10–12] at 809 and 718 cm^{-1}. Bands attributed to the stretching mode of terminal W=O bonds of the WO_x clusters are observed at 988 cm^{-1} [10, 11, 13]. The peak at 650 cm^{-1} corresponds to the tetragonal zirconia [10]. This result indicates that WO_3 and polymeric tungstate domains coexist on the surface of the cWZ-1-923 samples.

The Raman spectra of the ion-exchanged cWZ-2-923 samples (Fig. 5b) possess badly defined bands at 990 (shoulder), 955 and 850 cm^{-1}. The former two bands are characteristic of W=O stretching vibrations of W=O groups within the WO_x clusters, whereas that at 850 cm^{-1} is attributed to the ν_{as}(W-O-W) mode [10, 11, 13]. The comparison with the spectra of the as prepared samples (Fig. 4b) shows that the intensities of the bands at 850 cm^{-1} have increased relative to those at 955 cm^{-1}. This indicates that the crystallization of zirconia causes agglomeration of the WO_x clusters leading to increase in the number of W-O-W linkages. Since the spectra are recorded under ambient conditions, the adsorbed water causes broadening and low frequency shift of the W=O band [10, 11]. The large envelop with maximum at 955 cm^{-1} suggests the presence of various WO_x species with different degree of hydration. The shoulder at approximately 880 cm^{-1}, observed in the spectrum of the WZ-I sample (Fig. 5b, spectrum d), is assigned by Scheithauer et al. [10] to the W-O-Zr stretching mode. This band is not resolved for the ion-exchanged cWZ-2-923 materials. No peaks characteristic of WO_3 are detected for the samples with surface densities ranging from 4.9 to 5.3 W atoms/nm^2 (samples 0.05WZ-2-923, 0.50WZ-2-923 and WZ-I). However, formation of WO_3 is observed in the 0.75WZ-2-923 and 0.90WZ-2-923 (surface densities of 5.8 W/nm^2) which is concluded from the appearance of bands at 716 and 808 cm^{-1} (the spectrum of the 0.90WZ-2-923 sample is identical to that of the 0.75WZ-2-923 sample and it is not shown).

In situ FT-IR spectroscopy

This technique was used to characterize the structure of the dehydrated cWZ-2-923 materials. The FT-IR spectra of the samples show different patterns in the ν(OH) stretching region (Fig. 6a). The spectrum of the 0.05WZ-2-923 sample (surface density of 5 W/nm^2) exhibits very strong

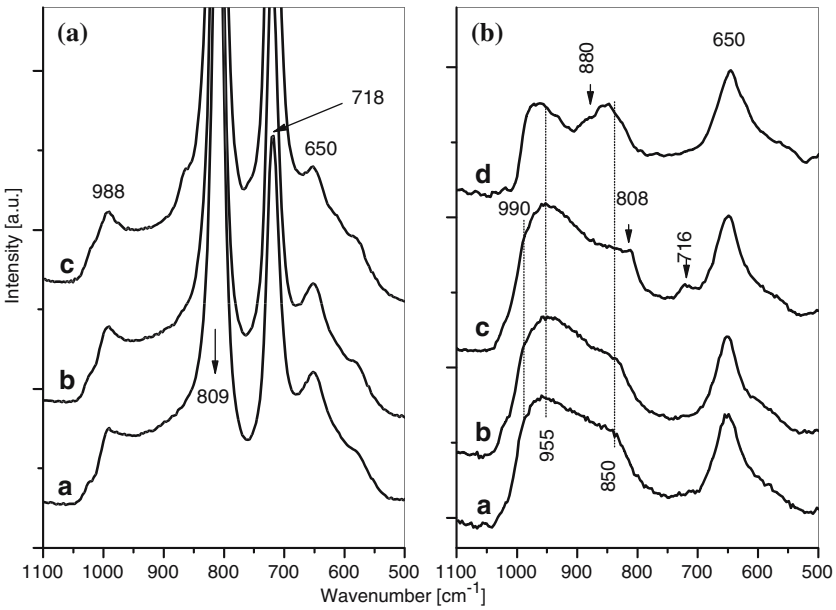

Fig. 5 Raman spectra of the calcined samples. Panel **a**: (a) 0.050WZ-1-923, (b) 0.50WZ-1-923, and (c) 0.75WZ-1-923. Panel **b**: (a) 0.050WZ-2-923, (b) 0.50WZ-2-923, (c) 0.75WZ-2-923 and (d) WZ-I. The spectra are normalized to the tetragonal zirconia band at 650 cm^{-1}

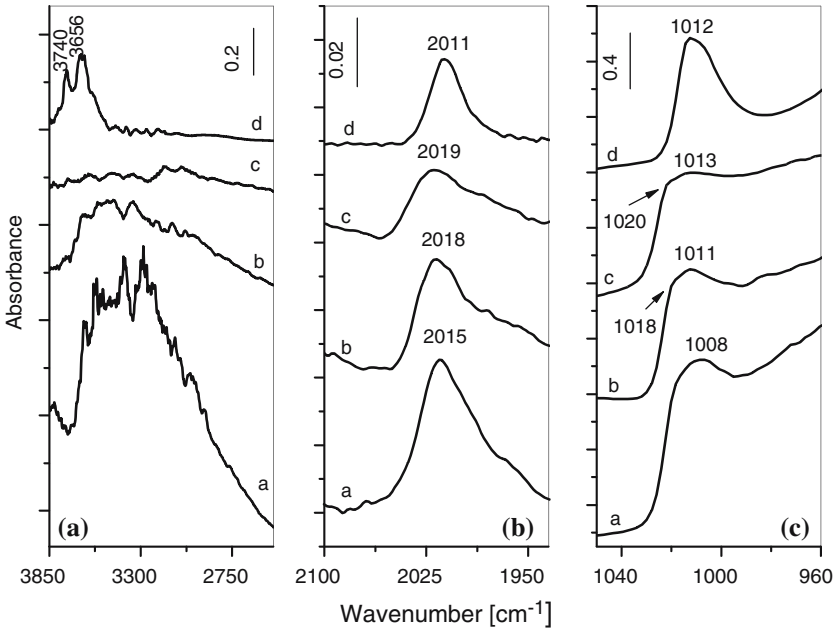

Fig. 6 FT-IR spectra in the OH stretching region (panel **a**), first W=O overtone region (panel **b**) and fundamental W=O stretching region (panel **c**) of (a) 0.050WZ-2-923, (b) 0.50WZ-2-923, (c) 0.75WZ-2-923 and (d) WZ-I

absorption between 3620 and 2600 cm^{-1}. This indicates that this material is characterized by a high population of W–OH groups [6, 10]. No absorption corresponding to residual OH groups of zirconia is detected. The latter give rise to absorption bands above 3600 cm^{-1} [34–36] . At surface coverage of 5.3 W/nm^2 (sample 0.50WZ-2-923, spectrum b) the intensity of the band in the ν(OH) stretching region decreases significantly and it becomes very weak in the spectrum of the 0.75WZ-2-923 sample (Fig. 6a, spectrum c). The latter sample has the highest W loading (5.8 W/nm^2). The spectrum of the impregnated WZ-I material has two sharp bands at 3740 and 3652 cm^{-1} (Fig. 6a, spectrum d). The band at 3752 cm^{-1} is characteristic of the terminal Zr–OH groups of tetragonal zirconia [35]. Based on the shift observed upon CO adsorption at 80 K (see below), the band at 3656 cm^{-1} is assigned to W–OH groups. The spectrum of the impregnated sample in the fundamental W=O stretching region (Fig. 6c, spectrum d) shows a band at 1012 cm^{-1} which gives a single W=O overtone vibration at 2012 cm^{-1}. These are the typical spectral features corresponding to surface monoxo W=O species [10, 37]. The spectra of the dehydrated ion-exchanged samples in the 1050–950-cm^{-1} region (Fig. 6c) have profiles that differ from that of the impregnated material and they show dependence on the tungsten loading. With increasing the surface density of W, the maximum of the main band shifts to higher frequency with simultaneous decrease in the intensity. This indicates that progressive condensation of the WO_x domains takes place causing the decrease in the number of terminal W=O species. A close inspection of the spectra shows that the W=O band of the ion-exchanged samples is split containing shoulders at 1018–1020 cm^{-1} and a wide and flat signal between ca. 1000 and 960 cm^{-1}. Only the high-frequency components produce overtone bands at 2015–2019 cm^{-1}. The latter vibrations display asymmetries toward lower frequencies. This and the fact that the absorption in the 1000–960 cm^{-1} region is absent in the spectrum of the impregnated sample may indicate that the adsorption of metatungstate ions in the presence of H_2O_2 results in a much broader distribution of various WO_x species having different W=O bond orders. Two- and three-dimensional WO_x overlayers may coexist on the surface of zirconia as postulated by Scheithauer et al. [10] for high W loadings.

The intensities of the absorption in the OH region in the spectra of the ion-exchanged samples parallel the intensities of the W=O bands. This indicates that the OH coverage of the activated samples is associated with hydroxyls produced by dissociative adsorption of ambient water on coordinatively unsaturated (cus) W=O groups [38]. The OH groups complete the coordination sphere of the W=O species and give rise to Brønsted acid sites [38]. Since the number of the cus W=O species decreases with the increase in the W coverage, the amount of the W-OH groups decreases as well.

Characterization of the acid sites of tungstated zirconia by FT-IR spectroscopy of adsorbed CO at low temperature

The 0.05WZ-2-923 and WZ-I samples have identical tungsten density. However, the FT-IR spectra show significant difference in their degree of hydroxylation.

Furthermore, the spectra of these samples display different features in the W=O fundamental and overtone region. Therefore, we studied the adsorption of CO at the temperature of liquid nitrogen, which is well known to characterize both Lewis and Brønsted acid sites on a solid surface. Three types of CO interactions with the surface of tungstated zirconia are reported to take place giving rise to absorption bands at ca. 2190, 2163–2164 and 2142–2143 cm^{-1} [6, 10, 34]. They are characteristic of CO adsorbed on coordinatively unsaturated (cus) Zr^{4+} sites, H-bonding interactions with acidic hydroxyl groups and physisorbed CO, respectively. At 77 K, CO is irreversibly bonded to the cus Zr^{4+} sites and the complex band at ca. 2190 cm^{-1} resists prolonged evacuation [34]. No evidence is found for CO bonded to cus W^{6+} species of tungstated zirconia [6, 10, 34], which in the case of WO_3/SiO_2 [34] and WO_3/TiO_2 [39] are shown to give rise to carbonyl bands above 2200 cm^{-1}.

Absorption bands similar to that reported in the literature [6, 10, 34] are observed in the carbonyl region of the spectra of the 0.05WZ-2-923 and WZ-I samples obtained at 80 K upon introduction of incremental doses of CO (Fig. 7a, spectra 1a - 1g and 2a-2d). On the 0.05WZ-2-923 sample, the Zr^{4+}-CO bands are detected at 2191 and 2183 cm^{-1} after the admission of the first dose ensuring pressure of 0.05 mbar (Fig. 7a, spectrum 1a). These two bands become unresolved at 2190 cm^{-1} for higher CO pressures and saturate at 0.3 mbar (Fig. 7a, spectrum 1d). The growing signal at 2170 cm^{-1} indicates the interaction of CO with Brønsted acid sites. It broadens and shifts down to 2160 cm^{-1} at 8-mbar saturation pressure of CO (the spectrum not shown). The low-frequency component at 2144 cm^{-1} detected as a shoulder at higher pressures corresponds to a physisorbed CO [6, 10, 34]. The spectrum in the OH region taken under equilibrium CO pressure of 2.5 mbar (Fig. 6b) shows the perturbation of the surface W–OH hydroxyls. The adsorption of CO erodes the shoulder at ca. 3640 cm^{-1} and the maxima of the remaining bands shift to lower frequencies due to formation of OH-CO complexes [6, 10, 34].

The WZ-I sample contains also exposed Zr^{4+} ions giving rise at a low pressure of a carbonyl band at 2191 cm^{-1} (Fig. 7a, spectrum 2a). This band broadens and shits to lower frequency upon increasing doses of CO (Fig. 7a, spectra 2b–2f). Compared to the 0.05WZ-923 sample, the Zr^{4+}-CO species require higher pressure of CO (0.6 mbar) to be saturated. The band corresponding to the ν(CO) stretching vibration of the OH-CO complex initially observed at 2164 cm^{-1} (Fig. 7a, spectrum 2a) shifts to 2158 cm^{-1} after saturation at 5 mbar of CO pressure. In the ν(OH) stretching region (Fig. 7b, spectra 2 and 2′), the adsorption of CO under these conditions induces shift of the band at 3740 cm^{-1} by ca. 20 cm^{-1} characteristic of the terminal hydroxyls of pure zirconia [6, 34, 36]. The relatively sharp band at 3660 cm^{-1} is no longer present and a broad absorption appears centered at approximately 3550 cm^{-1}. The $\Delta\nu$(OH) value is about 110 cm^{-1} and corresponds to the perturbation of acidic W-OH groups caused by the weak base CO [6, 10].

For both samples the outgassing at the adsorption temperature (Fig. 7a, spectra 1h–1j and 2g, 2h) causes disappearance of the ZrOH–CO band and leaves the Zr^{4+}-CO bands shifted to 2199 cm^{-1}. The evacuation restores the original spectra in the OH stretching region.

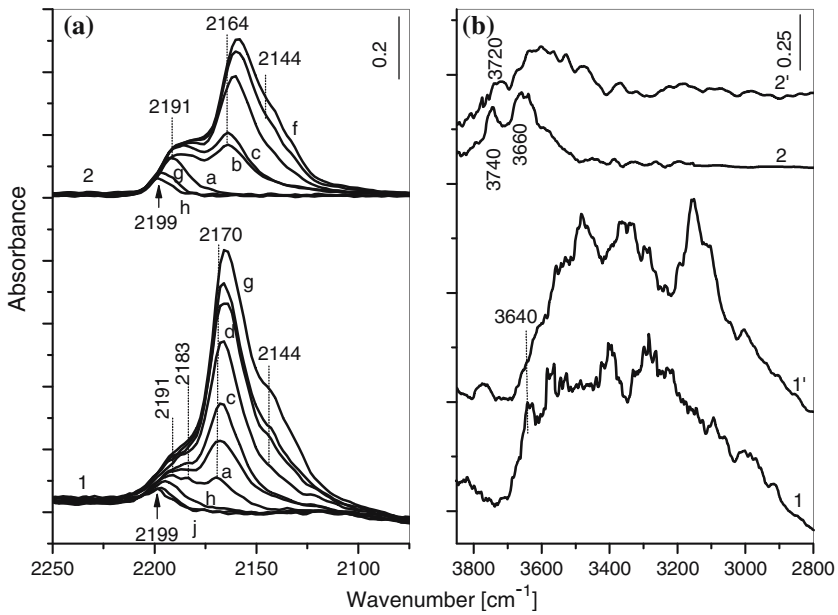

Fig. 7 FT-IR spectra of CO adsorbed at 80 K. Panel **a**: Spectra in the ν(CO) region of (1) sample 0.05WZ-2-923 upon increasing pressures of CO from (a) 0.05 mbar to (f) 0.6 mbar and (h to j) upon dynamic evacuation for a period of 30 min, and (2) sample WZ-I upon increasing pressures of CO from (a) 0.10 mbar to (f) 5.0 mbar and (g, h) upon dynamic evacuation for a period of 30 min. Panel **b**: Spectra in the ν(OH) stretching region of (1) sample 0.05WZ-2-923 before CO adsorption and (1′) under 2.5 mbar CO, and (2) sample WZ-I before CO adsorption and (2′) under 5 mbar CO

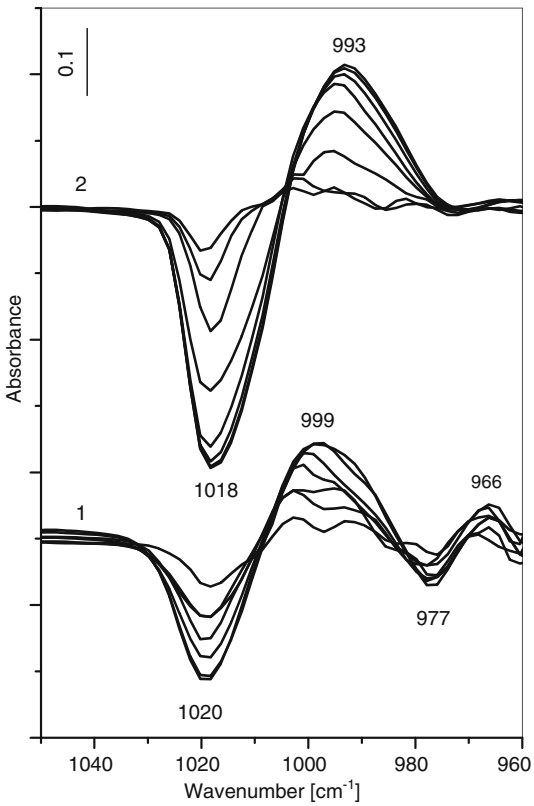

Fig. 8 Low-temperature FT-IR spectra in the W=O stretching region after adsorption of increasing pressures of CO on (1) sample 0.05WZ-2-923 and (2) sample WZ-I. The spectra of the activated samples before the admission of CO are subtracted

Knözinger and coworkers [6, 10] have shown that the adsorption of CO on Zr^{4+} sites at 80–85 K affects the W=O stretching modes of the neighboring polytungstate species. The latter vibration shifts to lower frequency due to inductive effects by the adsorbed CO. Figure 8 shows the perturbation of the W=O stretching modes of the 0.05WZ-1-923 and WZ-I samples observed at 80 K upon increasing pressures of CO. In the case of the ion-exchanged sample the adsorbed CO affects two W=O bands at 1020 and 977 cm^{-1} which shift to 999 and to 966 cm^{-1}, respectively. On the WZ-I sample only one band at 1018 cm^{-1} is perturbed.

Discussion

The Raman spectra of the equilibrated solutions have shown that the adsorbing species in solution 1 are the $[W_2O_3(O_2)_4(H_2O)_2]^{2-}$ ions. Although some amount of these ions has been formed in the equilibrated solution 2, the predominant species in this solution are the metatungstate ions, $[H_2W_{12}O_{40}]^{6-}$. Valigi et al. [14] concluded that the size of the metatungstate anion is comparable with the main micropore radius of amorphous zirconia. Because the size of the metatungstate ion is larger than that of the peroxo complex, limited adsorption from solution 2 occurs which lowers the uptake. The W surface densities in the as prepared samples using solutions 1 and 2 as precursors have been determined in the range of 3.4–3.5 and 2.4–2.6 W/nm^2, respectively. The latter value is higher than that reported in the literature (0.4 W/nm^2) for a system obtained by equilibrium adsorption from aqueous non-peroxide solutions at pH 2 using hydrated zirconia as a starting material [14, 15].

Two main interactions between the surface of the amorphous zirconium oxyhydroxide and the anionic precursors at pH 1.8 can be considered. The first interaction can be described mainly in terms of electrostatic attraction. It is known that in very acidic media (below the isoelectric point of zirconia), the hydroxyls of the support are protonated and they can act as anion adsorption sites [18]. This step for the $[W_2O_3(O_2)_4(H_2O)_2]^{2-}$ precursor anion is schematically depicted below (Step 1):

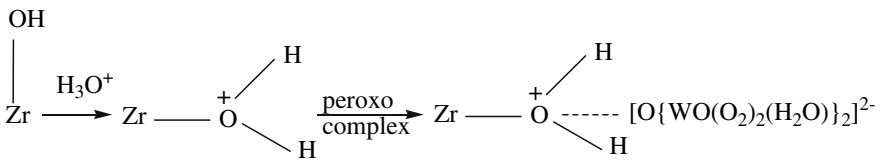

Step 1

The second interaction involves a chemical reaction, which leads to increase in the amount of the protonated OH groups and to the formation of surface heteroperoxo complexes (Step 2):

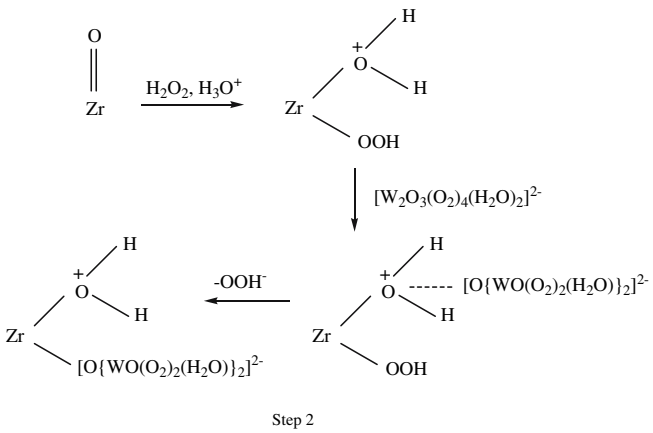

Step 2

The generation of additional protonated hydroxyls combined with the reduced nuclearity of the precursor ions enhances the ion-exchanged capacity of the support.

Formation of surface $Zr(O_2)$ species is confirmed by the Raman spectrum of the H_2O_2-treated ZrO_2-383 sample (Fig. 4). These species are stable and they are present on the sample dried at 383 K. However, the $Zr(O_2)$ groups in the as prepared cWZ-1-383 samples are either absent or their amount is low. This suggests that the Zr(IV) peroxo species are replaced by the adsorbed $[W_2O_3(O_2)_4(H_2O)_2]^{2-}$ ions. The latter most likely undergo degradation and rearrangement to polytungstates during the drying at 383 K. The same adsorption scheme can be proposed for the metatungstate ions. However, the different types of the adsorbing anions present in solutions 1 and 2 establish different equilibria, which control the uptake.

Furthermore, the Raman data show presence of dissolved Zr^{4+} ions in the acidic H_2O_2 solution in equilibrium with the hydrous zirconia (Fig. 1b, spectrum a′). One may hypothesize that the partial solubility of the support can favor the formation of Zr-containing polytungstates on the surface of the support. Carrier et al. [40] observed the formation of Anderson-type aluminum heteroplymolybdates on the surface of MoO_x/γ-Al_2O_3 catalyst prepared by equilibrium adsorption from heptamolybdate solution. In the light of these considerations, the structure of the WO_x species of the cWZ-383 samples of the two series can be envisioned as Zr-containing polytungstates as first proposed by Scheithauer et al. [10].

It can be concluded from the Raman spectra of the calcined samples that the deposition of WO_x species on zirconia by equilibrium adsorption from H_2O_2 solutions of $(NH_4)_2WO_4$ and AMT at pH 1.8 gives better results for the metatungstate precursor. The W loading on the amorphous support that is achieved by adsorbing the dimeric oxo-diperoxo anion is high enough to exceed the monolayer capacity of zirconia after the crystallization. As a result, polytungstate domains coexist with crystalline WO_3. Loridant et al. [22] did not observe WO_3 on their calcined samples prepared by ion exchange from the same peroxo precursor. The reason for this difference could be the short adsorption time employed in their synthesis (15 min).

According to the Raman spectra, the cWZ-2-923 samples with surface density of 5.0–5.3 W/nm^2 and the impregnated WZ-I material do not contain microcrystalline WO_3. The FT-IR spectra of CO adsorbed at 80 K indicate that the method of preparation (equilibrium adsorption versus impregnation) affects the extent of occupation of the Lewis acid sites of zirconia by the WO_x species and the amount and strength of the Brønsted acid sites. The 0.05WZ-2-923 and WZ-I samples have identical W density. However, the fact that the saturation of the Zr^{4+} ions of the 0.05WZ-2-923 sample by the adsorbed CO requires lower pressure suggests that the fraction of the WO_x-free surface is lower in the ion-exchanged than in the impregnated material. On the other hand, the OH-CO band of the 0.05WZ-2-923 sample is at higher frequency and requires higher pressure of CO to be saturated than that of the WZ-I sample. This indicates [6, 10] that the amount and the strength of the Brønsted acid sites are higher on the ion-exchanged than on the impregnated material. According to the DR–UV–vis data, the average size of the WO_x domains on both samples is identical. However, the polytungstate overlayer on the ion-exchanged and impregnated samples may differ by the amount of Zr-containing polytungstates. The fact that the spectra of the ion-exchanged cWZ-2-923 samples exhibit absorption in the 1000–960 cm^{-1} region (which is absent in the spectrum of the impregnated material) could support this assumption. This absorption may originate from WO_x clusters in which the W–O–Zr linkages to the support predominate. Eibl et al. [29] concluded that these species give rise to W=O bands at low frequency. Recently, Carrier and co-workers [41, 42] suggested Lindqvist-type units, $[ZrW_5O_{18}]^{2-}$, as molecular analogues of zirconia-supported tungsten catalysts. The authors showed that the IR spectrum of the $[W_6O_{19}]^{2-}$ anion displays strong and symmetric ν_s(W=O) band at 996 cm^{-1}. Substituting W with Zr causes this band to split and to shift to lower frequency (972–965 cm^{-1}) [41, 42]. The FT-IR spectroscopic investigation of CO adsorbed at 80 K on the 0.05WZ-2-923 sample shows the perturbation of two bands at 1020 and 977 cm^{-1} after exposure to increasing pressures of the probe molecule, whereas only one band at 1018 cm^{-1} of the impregnated sample is affected by the adsorbed CO (Fig. 8). Therefore, we infer that the negative absorption at 977 cm^{-1} in Fig. 7 corresponds to the W=O stretching modes of Zr-containing polytungstates which are perturbed by the adsorbed CO. These heteropolytungstates (surface pseudo-hetropoly anions) proposed already by Scheithauer et al. [10] are responsible for the acidity of tungstated zirconia. Incorporation of Zr^{4+} ions into the $(WO_6)_x$ network requires

charge-compensation by protons generating permanent Brønsted acidity [6, 10]. The formation of Zr-containing polytungstates on the ion-exchanged sample is favored by the partial solubility of hydrous zirconia in the H_2O_2 solution. This probably occurs to a smaller extent in the course of impregnation of the support with an aqueous solution of AMT.

Conclusions

Two series of WO_x/ZrO_2 samples are prepared by equilibrium adsorption from H_2O_2 solutions at pH 1.8 containing two different precursor anions, $[W_2O_3(O_2)_4(H_2O)_2]^{2-}$ and $[H_2W_{12}O_{40}]^{6-}$. The starting material is amorphous zirconium oxyhydroxide. The maximum surface densities of the deposited WO_x species are larger than that reported in the literature for systems obtained by the same technique using aqueous non-peroxide solutions. In the case of the metatungstate precursor, this increase is attributed to the generation of large amount of protonated hydroxyls (acting as anchoring sites) by the interaction between the amorphous support and H_2O_2. For the peroxo complex, the increase in the uptake is associated with both the $ZrO_x(OH)_{4-2x}$-H_2O_2 interaction and low nuclearity of the adsorbing anion.

The molecular structure of the materials is examined by DR–UV–vis, Micro-Raman and in situ FT-IR spectroscopy. The results are interpreted in terms of the increased polymerization of WO_x species with increasing the concentration of the precursor solutions, respectively the W loading. All materials obtained by adsorbing the $[W_2O_3(O_2)_4(H_2O)_2]^{2-}$ ions contain crystalline WO_3 after the calcination at 923 K. In contrast, this compound does not form on the calcined samples with loading of 5.0–5.3 W/nm^2 prepared from the $[H_2W_{12}O_{40}]^{6-}$–H_2O_2 precursor solutions. The FT-IR spectra of CO adsorbed at 80 K indicate that the method of preparation (equilibrium adsorption from the $[H_2W_{12}O_{40}]^{6-}$-H_2O_2 system versus impregnation with aqueous solution of ammonium metatungstate) affects the extent of occupation of the Lewis acid sites of zirconia by the WO_x species and the amount and strength of the Brønsted acid sites. For materials with identical W loading, the fraction of the WO_x-free surface is higher on the impregnated sample than that on the sample obtained by equilibrium adsorption from the $[H_2W_{12}O_{40}]^{6-}$–H_2O_2 solution. It is proposed that the high Brønsted acidity of the ion-exchanged sample is associated with the existence of a substantial amount of Zr-containing polytungstates. Their formation is favored by the partial solubility of hydrous zirconia in the H_2O_2 solution.

Acknowledgements This work was financially supported by Bilkent University and the Scientific and Technical Research Council of Turkey (TÜBITAK), Projects 106T081 and 105M094.

References

1. Hino M, Arata K (1988) J Chem Soc Chem Commun 1259
2. Ono Y (2003) Catal Today 81:3
3. Iglesia E, Barton DG, Soled SL, MIESO S, Baumgartner JE, Gates WE, Fuentes GA, Meitzner GD (1996) In: Hightower JW, Delgass WN, Iglesia E, Bell AT (eds) Studies in surface science and catalysis, vol 101. Elsevier, Amsterdam, p 533
4. Barton DG, Soled SL, Meitzner DG, Fuentes GA, Iglesia EG (1999) J Catal 181:57
5. Santiesteban JG, Vartuli JC, Han S, Bastian D, Chang CD (1997) J Catal 168:431
6. Scheithauer M, Cheung T-K, Jentoft RE, Grasselli RG, Gates BC, Knözinger H (1998) J Catal 180:1
7. Kuba S, Lukinskas P, Grasselli RK, Gates BC, Knözinger H (2003) J Catal 216:353
8. Chin Y-H, Alvarez WE, Resasco DE (2000) Catal Today 62:159
9. Chin Y-H, Alvarez WE, Resasco DE (2000) Catal Today 62:291
10. Scheithauer M, Grasselli RK, Knözinger H (1998) Langmuir 14:3019
11. Kuba S, Concepcion Heydorn P, Grasselli RK, Gates BC, Che M, Knözinger H (2001) Phys Chem Chem Phys 3:146
12. Barton DG, Shtein M, Wilson RD, Soled SL, Iglesia E (1999) J Phys Chem B 103:630
13. Valigi M, Gazzoli D, Pettiti I, Matei G, Colonna S, De Rossi S, Ferraris G (2002) Appl Catal A 231:159
14. Valigi M, Gazzoli D, Cimino A, Proverbio E (1999) J Phys Chem B 103:11318
15. Gazzoli D, Valigi M, Dragone R, Marucci A, Mattei G (1997) J Phys Chem B 101:11129
16. Valigi M, Gazzoli D, Ferraris G, De Rossi S, Spinicci R (2005) Mol Catal A 227:59
17. Greenwood NN, Earnshaw A (2002) In: Chemistry of the elements. Butterworth & Heineman, Oxford, p 1010
18. Brunelle JP (1978) J Pure Appl Chem 50:1211
19. Vol'nov I (1987) In: Peroxide complexes of vanadium, niobium and tantalum. Nauka, Moscow, p 12
20. Dickman MH, Pope MT (1994) Chem Rev 94:569
21. Kantcheva M (2000) Phys Chem Chem Phys 2:3043
22. Loridant S, Feche C, Essayem N, Figueras F (2005) J Phys Chem B 109:5631
23. Kantcheva M, Ciftlikli EZ (2002) J Phys Chem B 106:3941
24. Crouthamel CE, Johnson CE (1954) Anal Chem 26:1284
25. Wood DF, Clark RT (1958) Analyst 83:326
26. Nakamoto K (1997) In: Infrared and Raman spectra of inorganic and coordination compounds. Part A. J. Wiley & Sons, New York, p 187
27. Nakamoto K (1997) In: Infrared and Raman spectra of inorganic and coordination compounds. Part A. J. Wiley & Sons, New York, p 182
28. Aubry C, Chottard G, Platzer N, Brègeault J-M, Thouvenot R, Chauveau F, Huet C, Ledon H (1991) Inorg Chem 30:4409
29. Eibl S, Gates BC, Knözinger H (2001) Langmuir 17:107
30. Weber RS (1995) J Catal 151:470
31. Keramidas VG, White WB (1974) J Am Ceram Soc 57:22
32. Nakamoto K (1997) In: Infrared and Raman spectra of inorganic and coordination compounds. Part B. J. Wiley & Sons, New York, p 157
33. Naito N, Katada N, Niwa M (1999) J Phys Chem B 103:7206
34. Ferraris G, De Rossi S, Gazzoli G, Pettiti I, Valigi M, Morterra C (2003) Appl Catal A 240:119
35. Jung KT, Bell AT (2000) J Molec Catal A 163:27
36. Hadjiivanov K, Lavalley J-C (2001) Catal Commun 2:129
37. Ramis G, Busca G, Cristiani C, Lietti L, Bregani F (1992) Langmuir 8:1744

38. Busca G (2002) J Raman Spectrosc 33:348
39. Eibl S, Fentoft RE, Gates BC, Knözinger H (2000) Phys Chem Chem Phys 2:2565
40. Carrier X, Lambert JF, Che M (1997) J Am Chem Soc 119:10137
41. Villanneau R, Carabineiro H, Carrier X, Thouvenot R, Herson P, Lemos F, Ribeiro FR, Che M (2004) J Phys Chem B 108:12465
42. Carabineiro H, Villanneau R, Carrier X, Herson P, Lemos F, Ribeiro FR, Proust A, Che M (2006) Inorg Chem 45:1915